INTERNATIONAL JOURNAL FOR NUMERICAL METHODS IN FLUIDS, VOL. 9, 9–22 (1989)

COMPARISON WITH EXPERIMENT FOR TVD CALCULATIONS OF BLAST WAVES FROM A SHOCK TUBE

CHARLIE H. COOKE

Old Dominion University, Norfolk, VA 23508, U.S.A.

AND

KEVIN S. FANSLER

U.S. Army Ballistic Research Laboratory, Aberdeen Proving Ground, Aberdeen, MD 21005, U.S.A.

SUMMARY

Harten's second-order-accurate total-variation-diminishing (TVD) scheme is applied to calculation of flow from the open end of a shock tube. Comparison of numerical results with available experimental data for overpressure at selected points around the shock tube exit shows good agreement. Numerically indicated positions of the moving shock front and Mach stem also compare well with flow shadowgraph data. Where the problem geometry is sufficiently simple and rectangular gridding can be used, Harten's method affords a good choice for blast wave calculations.

KEY WORDS Shock capturing Shock tube TVD scheme Compressible flow Fluid dynamics Comparison with experiment

INTRODUCTION

The purpose of this work is to test, and report upon, the numerical efficacy of Harten's[1] higher-order-accurate TVD scheme as applied to flow from a shock tube. This effort was motivated by a recent (TTCP) workshop to assess the current state of efficiency as regards calculation of blast overpressure.[2] The Harten scheme[1] is a total-variation-diminishing (TVD), second-order accurate and upwind-biased method for solving the Euler equations of compressible flow in one dimension. The method of operator splitting, first placed upon a sound analytical foundation by Strang,[3] permits application to higher dimensions and axisymmetric flow problems with preservation of second-order accuracy. The first author has established that the results of Strang can be extended so as to allow incorporation of source terms into the splitting.[4] More recently, the existence question for splittings which preserve higher-order accuracy has been investigated.[5] The details of the implementation of Harten's scheme employed here is well documented in Reference 6, with a paper by Yee and Kutler[7] providing clarifying background material. Boundary condition treatment, for the most part, follows the ideas of Widhopf *et al.*[8] Numerical results are compared with the experimental flow field surveys of Schmidt *et al.*[2,9]

0271–2091/89/010009–14$07.00

Received 25 November 1986
Revised 18 February 1988

SHOCK TUBE CONFIGURATION AND DESCRIPTION OF COMPUTATIONAL DOMAIN

The shock tube has an overall length of 3·717 m. The driver section is 0·673 m long, while the driven section is 3·044 m long. The tube is cylindrical, with an inside diameter of 0.152 m and outside diameter of 0.305 m. The thickness of the tube is larger than usual to avoid possible problems with implementing reflecting boundary conditions. Of course, tubes with thicker walls should result in the front part of the blast wave being stronger and the rear part of the blast wave being weaker. The exit diameter, $D = 0{\cdot}152$ m, is selected as reference length. The driver gas in nitrogen, while the driven gas is air at atmospheric pressure. The shock tube is operated with both sections initially at ambient temperature, 295 K. The driver is charged to a pressure of 1.67 MPa, producing a pressure behind the shock front at the tube exit of 342·0 kPa.

The simulation was performed on a VAX 11-780 computer system, with a uniform grid having a mesh density of 40 points per calibre. The calculation was run for 1·5 ms, sufficiently short to preclude the arrival of the contact surface at the tube exit; however, exit properties change for early times due to upstream propagation of a rarefaction wave as the flow expands. The computational domain, bounded below by the axis of symmetry, extends 3 calibres upstream, downstream and laterally from the tube exit. Time is referenced to zero when the shock exits from the tube. The front of the blast wave exits from the computational domain at about 1·0 ms; therefore the algorithm for the downstream continuation at the boundaries is important. The continuation used in the calculation will now be discussed briefly. As the Harten scheme has a five-point computational molecule, it can not be applied at the last two points near a boundary. At an outflow boundary, the point next to the boundary is therefore computed with a first-order-accurate flux using Godunov's method. The boundary value itself is then set to be the same as the value at the next-to-last point; this scheme is sometimes referred to as the supersonic outflow condition. No boundary reflections were observed to result from this method.

At the axis of symmetry, which is located at grid point 3, a reflection boundary condition is used. Values for points 4–5 immediately above the axis of symmetry are reflected to points 2–1 below, asymmetrically in the normal component of velocity; otherwise, symmetrically. Inflow conditions are held constant on the assumption that the contact surface, which was originally at the shock tube diaphragm, will not exit the barrel during the course of the calculation. The inflow origin is located well back within the barrel so as to allow for an expansion wave to travel back upstream. Wall boundaries are handled more or less in accordance with treatment of Reference 8.

NUMERICAL RESULTS

Contour data

The structure of jets has been discussed at length elsewhere.[10–12] We want to confirm that the numerical method is accurately simulating the blast wave generated by flow from the exit of a shock tube. We will compare pressure and Mach number contour plots with shadowgraph data. We will also compare the simulation overpressure time values with experiment. Pressure and Mach contours may be seen to compare with the shock and shear layer boundaries of the flow shadowgraphs of Schmidt *et al.*[2,9] Figures 1–3 show shadowgraphs obtained by Schmidt and the corresponding contour plots, which have the same scale as the shadowgraphs. Prssure and Mach number contours show the developing blast wave at 200, 500, 1000 and 1500 μs. Figure 1(a) is a shadowgraph of the upper part of the shock tube exit flow field 200 μs after exit of the blast wave from the shock tube. The tube exit plane is defined by the vertical boundary between the dark area

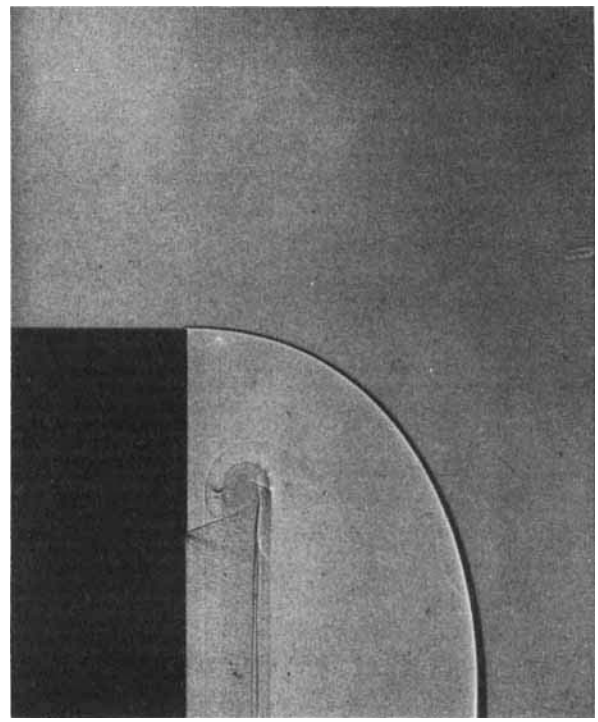

Figure 1(a). Shadowgraph of shock tube blast wave field at 200 μs

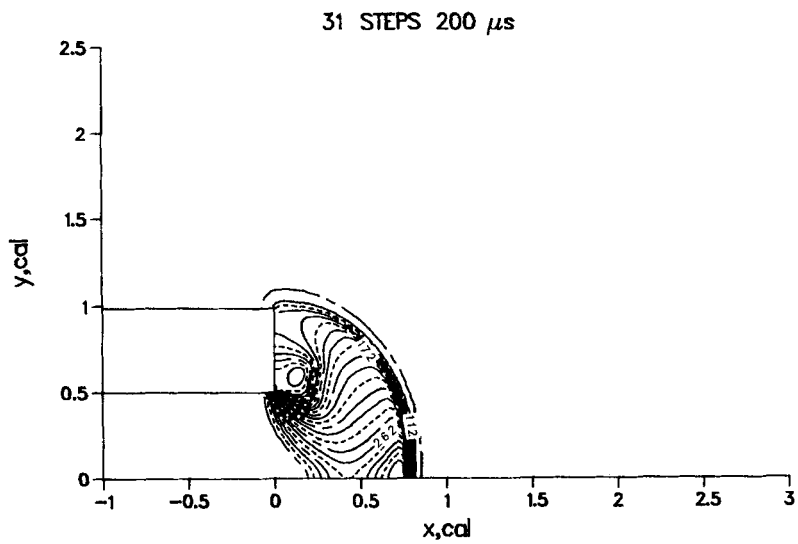

Figure 1(b). Shock tube pressure contours at 200 μs

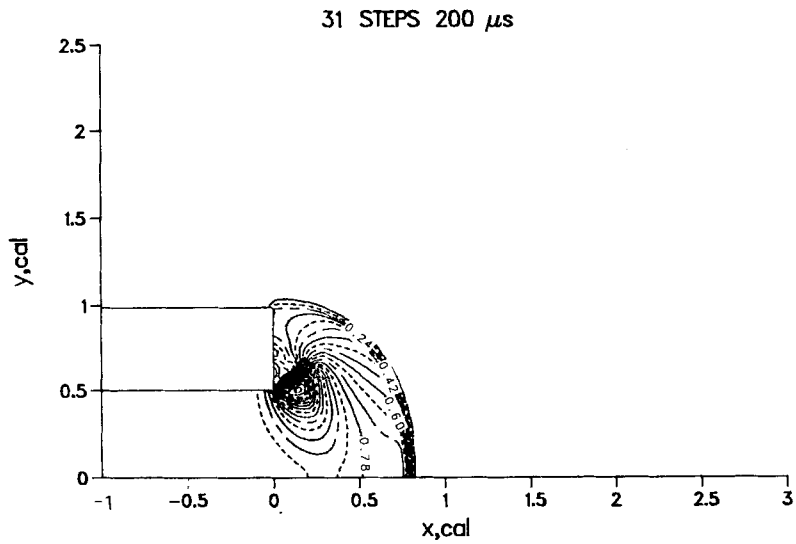

Figure 1(c). Shock tube Mach contours at 200 μs

to the left and the light area to the right. These shadowgraphs have been published elsewhere by Schmidt.[2] The oblique shock extends down and out from the tube exit corner to the backward-facing shock, which the shadowgraph shows as an almost vertical structure located near the exit. The shear layer and vortex formation are also shown and are discussed by Skews.[10] The general

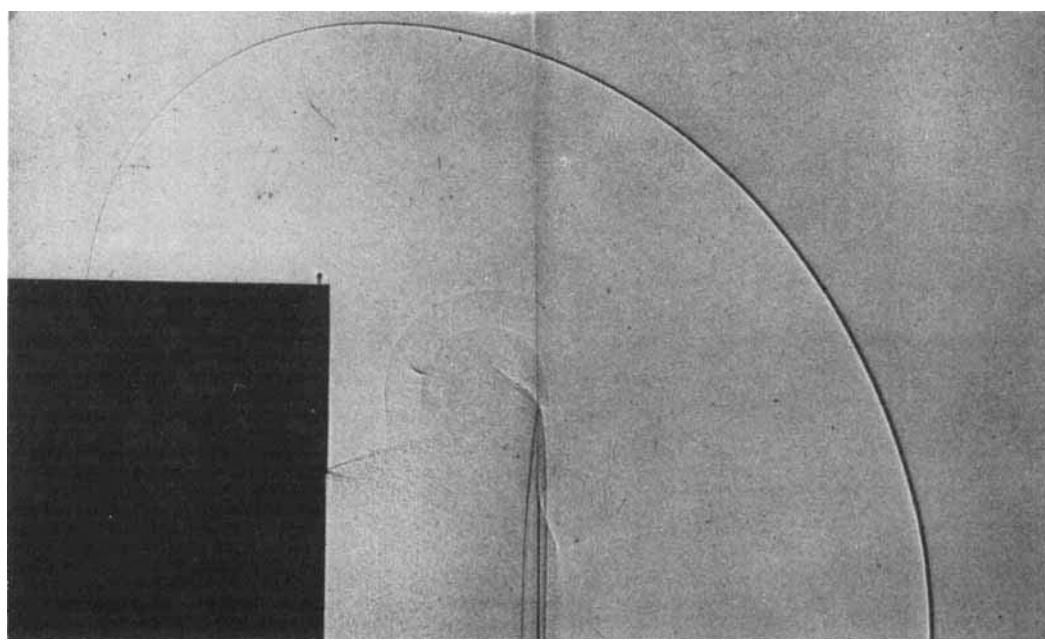

Figure 2(a). Shadowgraph of shock tube blast wave field at 500 μs

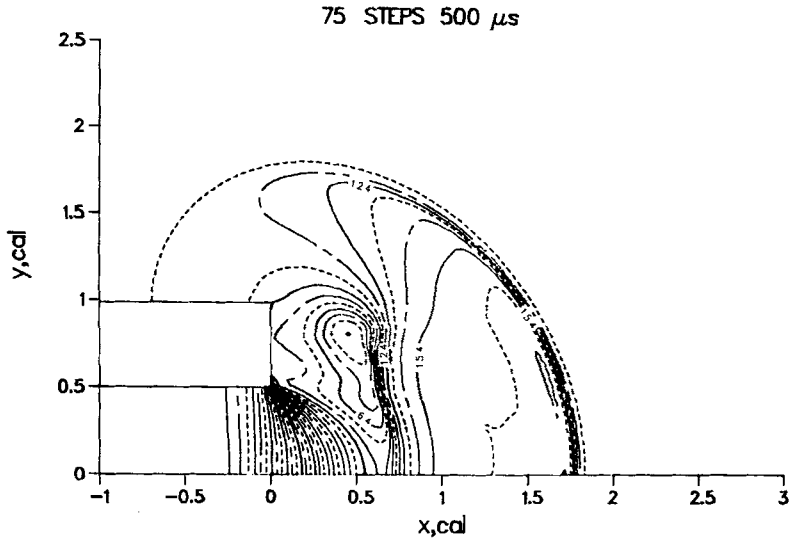

Figure 2(b). Shock tube pressure contours at 500 μs

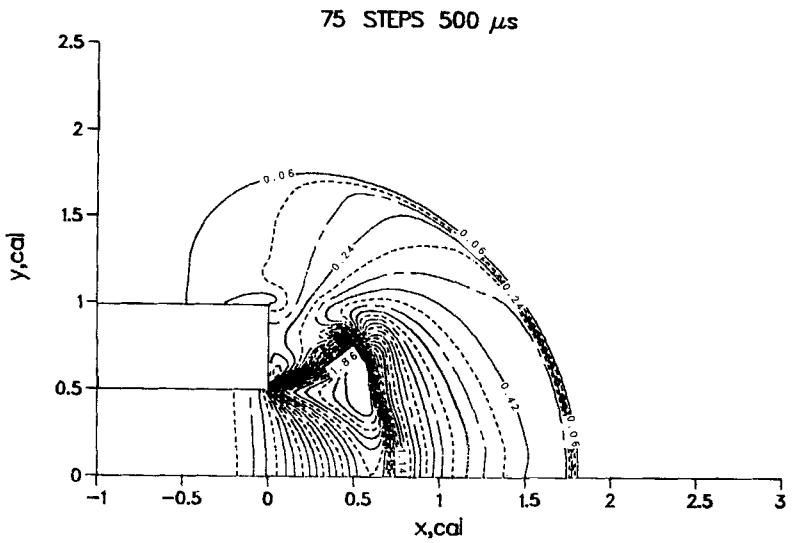

Figure 2(c). Shock tube Mach contours at 500 μs

behaviour of such vortices has also been discussed by Howard and Matthews.[13] The shear layer layer extends from the corner of the shock tube exit up and out to the backward-facing shock. The starting vortex can be seen above the shear layer and immediately behind the backward-facing shock. Figures 1(b) and 1(c) show respectively pressure contours and Mach contours at 200 μs. As with the shadowgraphs, only the upper half of the axisymmetric flow field is shown and the contour plots are scaled the same as the shadowgraphs. The co-ordinates are given in terms of calibres or inside diameters of the shock tube. The exit of the shock tube is at $x = 0$. The outside

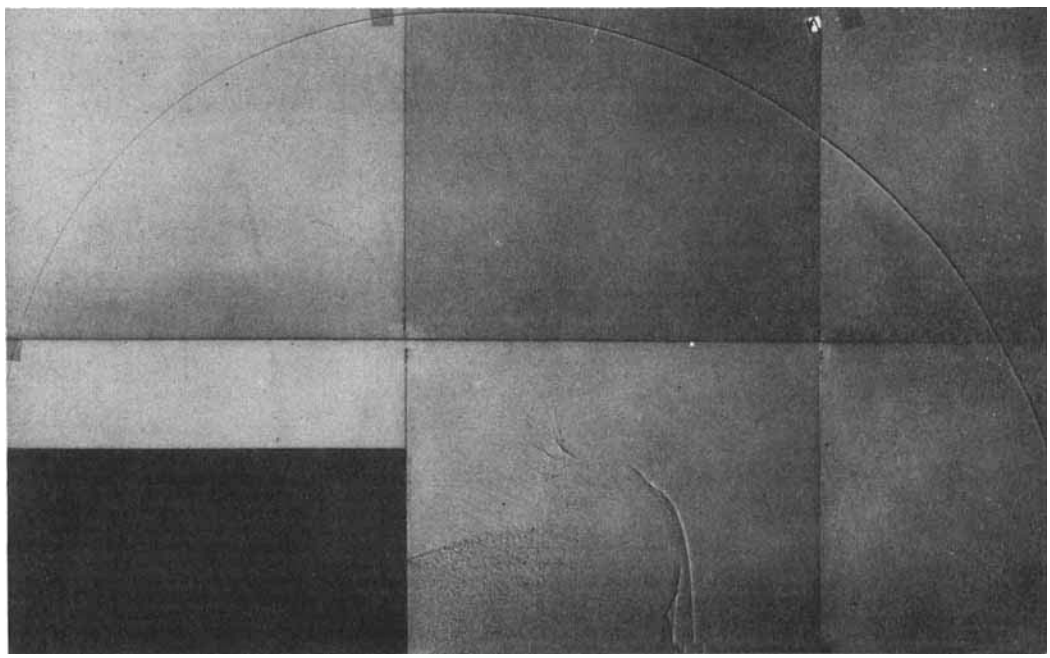

Figure 3(a). Shadowgraph of shock tube blast wave field at 1000 μs

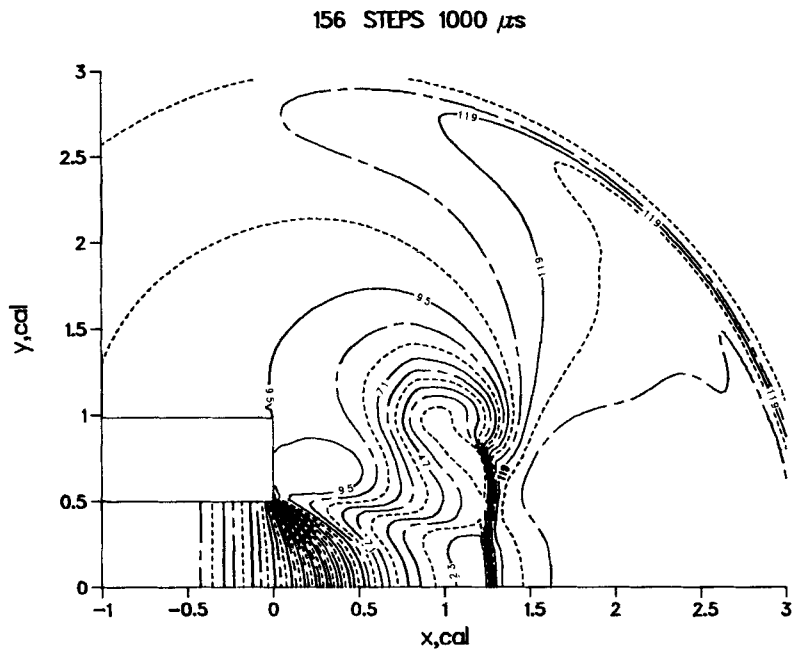

Figure 3(b). Shock tube pressure contours at 1000 μs

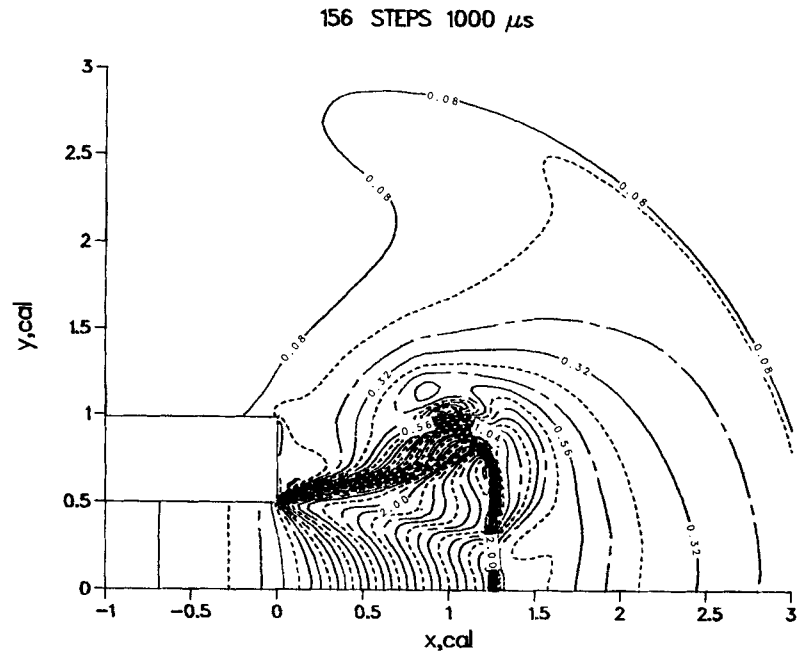

Figure 3(c). Shock tube Mach contours at 1000 μs

diameter of the shock tube is equal to two inside diameters of the shock tube. The upper, lower and right lines of the rectangle designate respectively the boundaries of the outside of the tube, the inside of the tube and the end of the tube. The solid, chain-dashed and dashed contour lines appear in sequence with increasing pressure or Mach value in order to improve the distinguishability of the contour lines at and near discontinuities. The overpressure values printed on the solid line contours are given in Pa. The flow at the shock tube exit is already clearly two-dimensional. Further, the Mach contour plot shows a shear layer developing up and out from the corner of the shock tube. The numerically obtained locations of the discontinuities agree well with experiment. Figure 2 shows the contour plots at 500 μs together with Schmidt's shadowgraph obtained for this time. At the centre of the shadowgraph is a vertical line that is the junction between the two pieces of film needed for displaying the upper part of the axisymmetric blast wave field. The backward-facing shock is clearly delineated, with the shear layer extending from the corner of the shock tube upward to the edge of the backward-facing shock. The front of the calculated blast wave has travelled out slightly farther than is observed. Figure 3 shows the contour plots and the corresponding shadowgraph at 1 ms. This shadowgraph was obtained with six pieces of photographic film placed next to each other. The oblique shock, shear layer and Mach disc are seen clearly in both the shadowgraph and the contour plots. The part of the inward-facing shock that is above its junction with the oblique shock is starting to bend over toward the axis. The shadowgraph shows that almost all the propellant flow is turbulent, particularly so in the shear layer. Figure 4 shows the contour plots at 1·5 ms. the Mach disc diminishes considerably in size and forms a junction with the oblique shock, the inward-facing shock that bends toward the axis and a shear layer that demarcates the flow passing through the Mach disc and the flow passing through the oblique shock and thence through the upper part of the inward-facing shock.

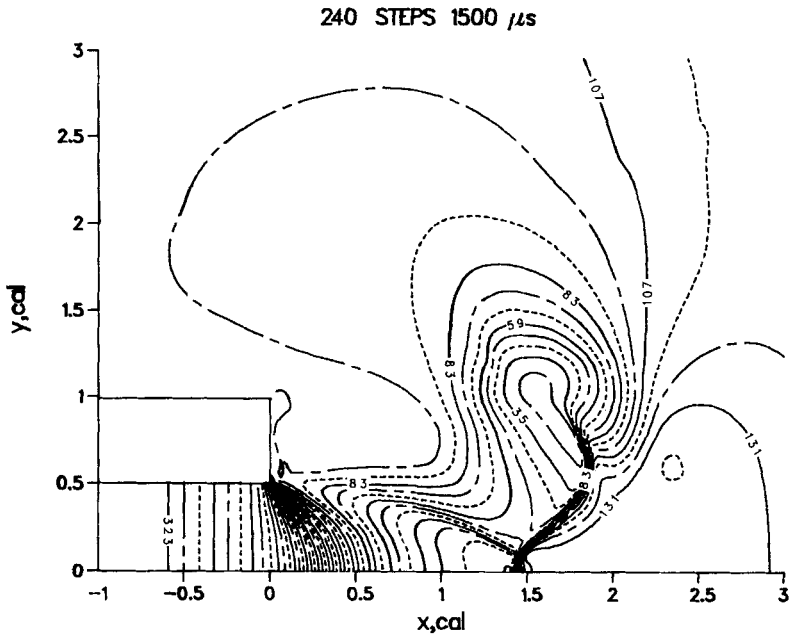

Figure 4(a). Shock tube pressure contours at 1500 μs

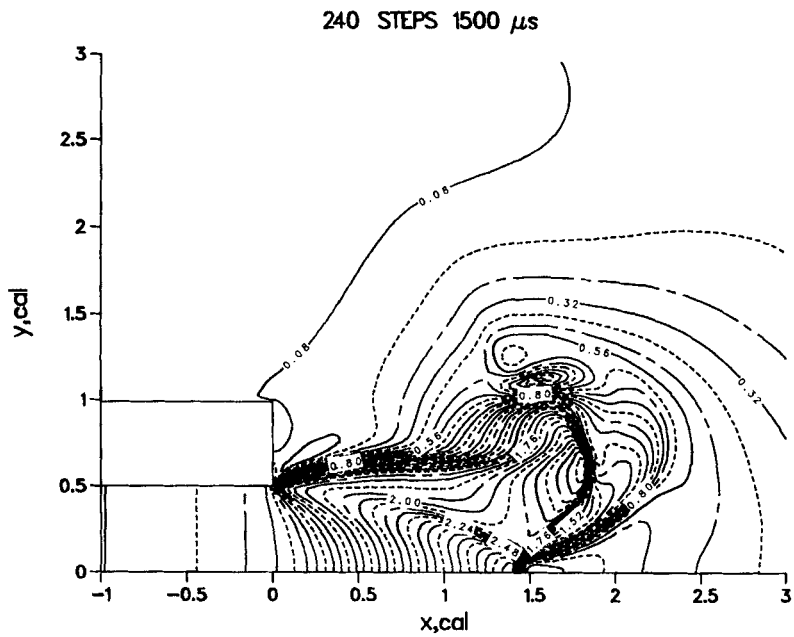

Figure 4(b). Shock tube Mach contours at 1500 μs

Although the corresponding shadowgraph for this time was not available for use in this paper, the structure shows substantial agreement with data of Schmidt.[2]

As noted before, Figures 2, 3 and 4 all show a vortex located above the shear layer, near the top edge of the inward-facing shock. This is the starting vortex, which for an inviscid flow is generated by a tangential discontinuity. Discontinuities such as shear layers and curved shocks cause instabilities; hence significant amounts of turbulence are created in flows from shock tubes and gun weapons. With this inviscid scheme, the simulated flow is non-turbulent but the locations of the discontinuities still agree well with the shadowgraph data. The simulated shear layers are a few grid points in thickness.

Overpressure time histories

Overpressure, density and Mach number time histories were recorded at points on a circle of radius 1·5D centred at the intersection of the axis of symmetry and the exit plane. The points were distributed at angles of 0°, 30°, 60°, 90°, 120° and 130°. Other measurement points were located 4·7 cm inside and on the barrel; on the face of the barrel and in the exit plane, 11.3 cm from the axis of symmetry; and finally, on the top and outside of the barrel, 8·26 cm upstream from the exit plane.

Figures 5–13 show comparisons of experimental and numerical overpressure time histories at these points. Agreement is generally good, but with some exceptions. Figure 5 exhibits data for the point on the axis 1·5D downstream from the exit plane; for times near 1500 μs experimental and numerical results differ drastically. Computations indicate that the inward-facing shock has not yet reached 1·5 calibres downstream from the muzzle, while experimental probe data show the opposite. However, shadowgraphs and further measurements indicate that, on the axis, interactions between the pressure probe and the shock induce oscillations in the jet flow and position of the Mach disc.[2] Figure 6 also shows disagreement for the time when the inward-facing shock reaches the position. It is conjectured that the interaction processes may also be occurring at this position. Another source of error stems from the way the experimental probes were simulated. The

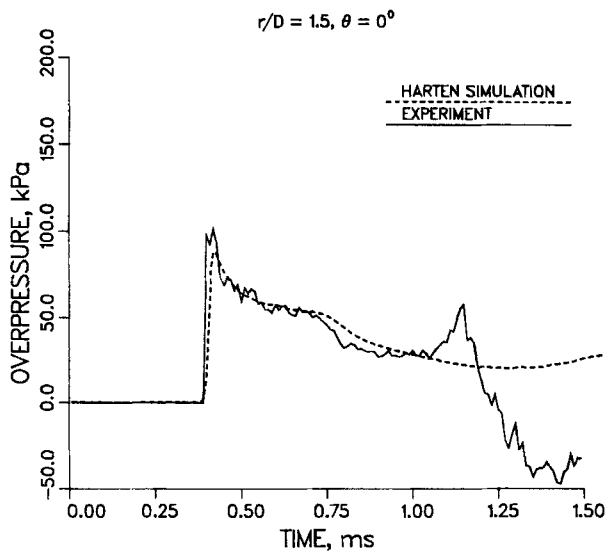

Figure 5. Pressure versus time, $r/D = 1{\cdot}5$, $\theta = 0°$

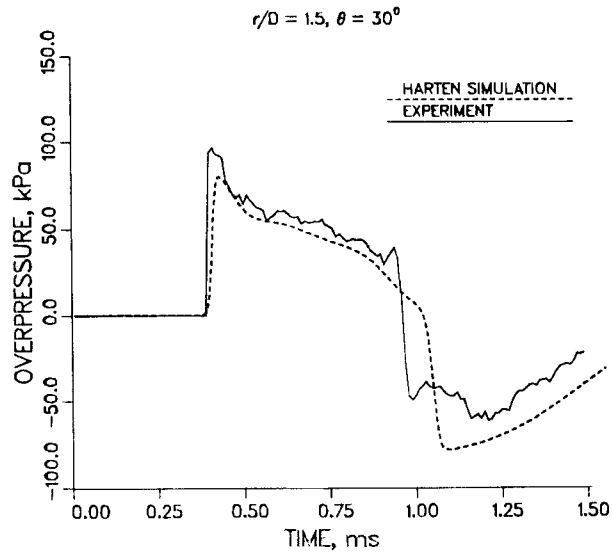

Figure 6. Pressure versus time, $r/D = 1.5$, $\theta = 30°$

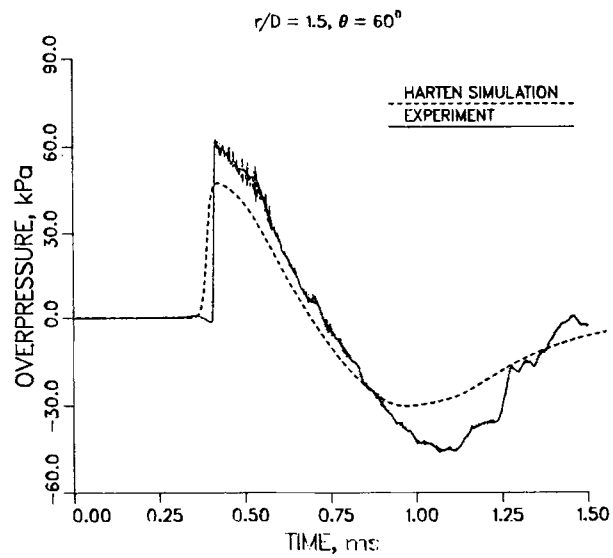

Figure 7. Pressure versus time, $r/D = 1.5$, $\theta = 60°$

grid point nearest the experimental point was selected for comparison in cases where interpolations would involve more than two points. For certain positions in the flow field, the location of the point might be critical for obtaining accurate simulation results. Here the numerical data were collected at a point a half-cell width away from the exit plane, but otherwise at proper elevation. Figure 12 is the overpressure comparison on the face of the shock tube exit. The time of arrival for the blast wave is most in disagreement at this location. However, if viscous effects are to cause

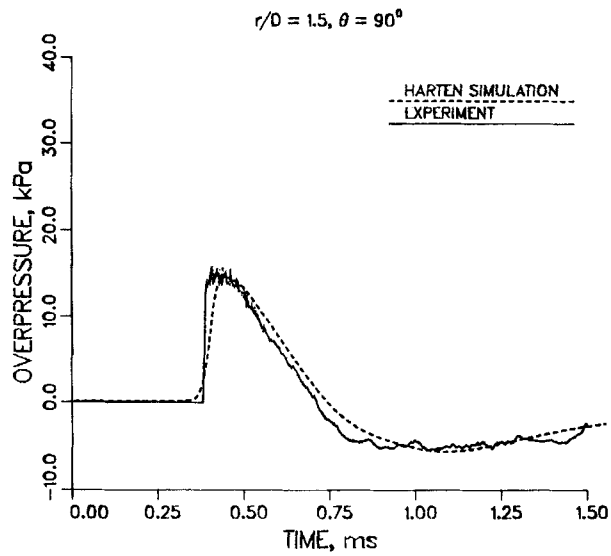

Figure 8. Pressure versus time, $r/D = 1.5$, $\theta = 90°$

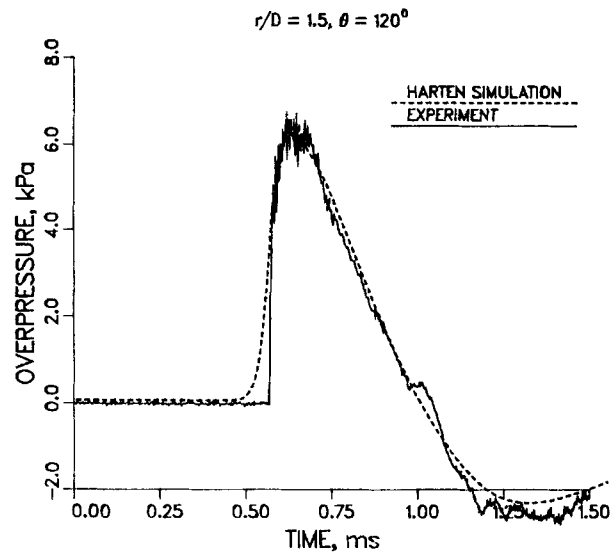

Figure 9. Pressure versus time, $r/D = 1{\cdot}5$, $\theta = 120°$

disagreement anywhere, this and other wall locations appear most likely. Figure 13 is a comparison of the overpressures on the outside of the tube. The experimental trace has an extraneous oscillatory signal superimposed upon it, perhaps caused by mechanical vibrations set up in the transducer. It is therefore difficult to assess the quality of the agreement for this position. From Figures 5–10, the shock front time-of-arrival values for experiment and simulation agree better at the field points in the back of the exit plane than at the forward field points. The contour

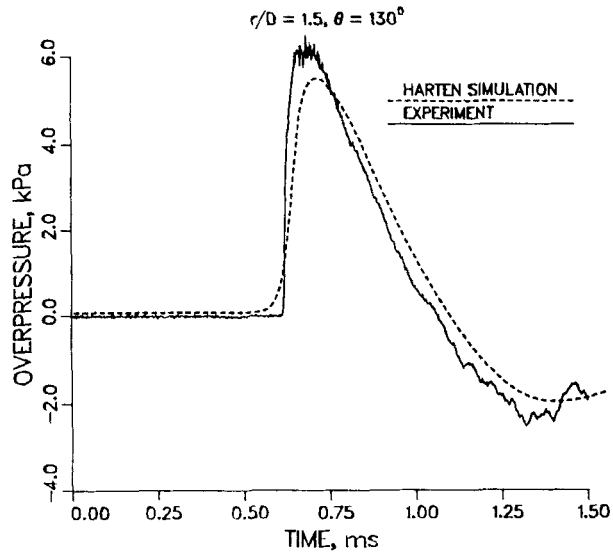

Figure 10. Pressure versus time, $r/D = 1.5$, $\theta = 130°$

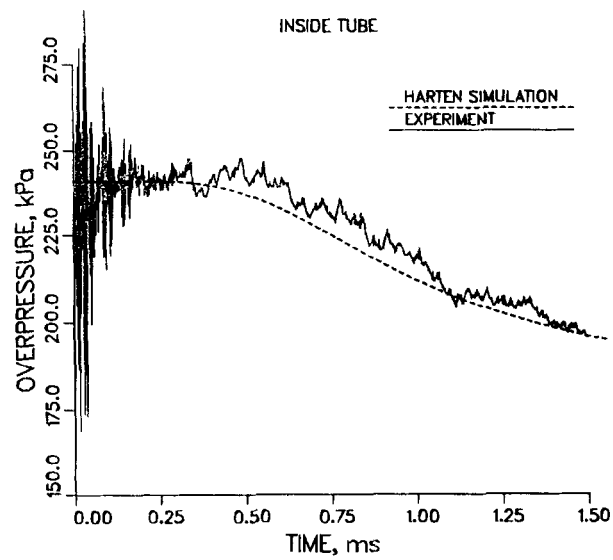

Figure 11. Pressure versus time for the shock tube at a location 0·3 calibres behind the muzzle on the inside surface of the tube

plots and shadowgraphs also yielded results that are consistent with the overpressure results. The present TVD scheme is a useful and valuable tool for obtaining and analysing transient shock structure. Moon and Yee,[14] using a Harten TVD scheme, also obtained good agreement with experiment where they simulated shock reflections from aerofoils at high angles of attack.

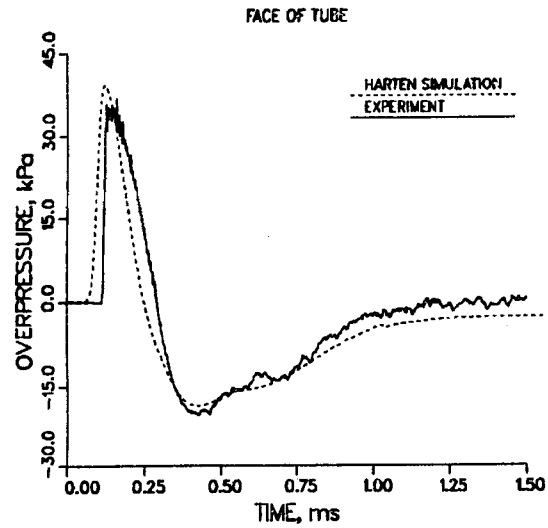

Figure 12. Pressure versus time at a point on the face of the shock tube, 0·74 calibres from the axis of symmetry

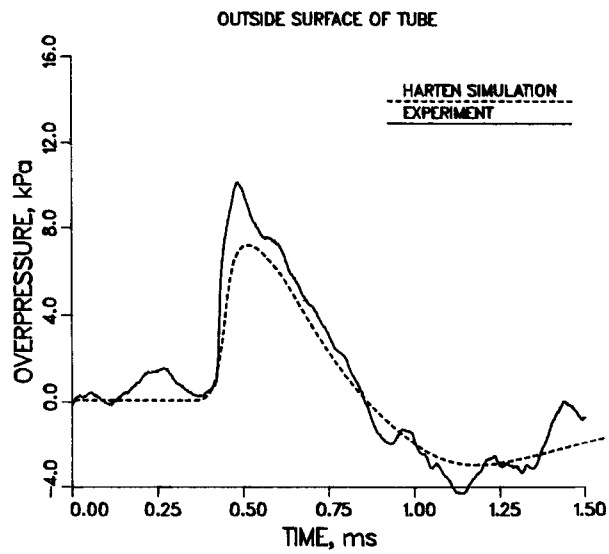

Figure 13. Pressure versus time at a location on the Barrel 0.54 calibres upstream from the exit plane of the shock tube

The peaks predicted by the simulation, with one exception, are less than experiment indicates. The agreement could be improved by further grid refinement. However, the computing resources were not available to perform the simulation with a finer grid. The use of artificial compression would also produce higher levels for peak pressures and crisper looking shocks. Nevertheless, the use of artificial compression has been avoided, as it is known to produce inaccuracies in regions of flow expansion.

SUMMARY AND CONCLUSIONS

The feasibility of calculating blast overpressures using Harten's TVD scheme has been assessed. Comparisons with experimental data show this method to be a good choice where a uniform grid can be tolerated. Numerical results compare well with both overpressure measurements and shadowgraph data. This implies that direction and speed of information flow are correctly maintained by the method, as used in conjunction with the usual operator splitting technique which accommodates higher dimensionality and the presence of source terms. This scheme has also been employed for simulating flow around axisymmetric silencers, with a bullet traversing through the field.[15] The method gives good results for smaller silencers, but for larger silencers the heat transfer to the device must also be simulated to obtain good accuracy. The Navier–Stokes equations are the method of choice for larger silencers since they can simulate the heat transfer as well as the gas viscosity. Of course, the price paid is more complexity and slower computing times.

REFERENCES

1. A. Harten, 'High resolution schemes for hyperbolic conservation laws', *J. Comput. Phys.*, **49**, 357–393 (1983).
2. E. M. Schmidt, *Proc. TTCP Workshop on Computation of Weapon's Launch Blast Over-Pressure, KTA-7*, Cincinnati, Ohio, 17 July 1985.
3. G. Strang, 'On the construction and comparison of difference schemes', *SIAM J. Numer. Anal.*, **5**, 506–517 (September 1968).
4. C. H. Cooke, 'On operator splitting for unsteady boundary value problems', *J. Comput. Phys.*, (December 1986).
5. C. H. Cooke, A. G. McMorran and S. A. Lowe, 'On the non-existence of few factor, higher-order accurate, fractional-step operator splittings for hyperbolic systems of conservation laws', submitted to *11th AIAA Symp. on Numerical Fluid Dynamics*, Williamsburg, Virginia, 29 May–2 June 1988.
6. C. H. Cooke, 'On operator splitting of the Euler equations consistent with Harten's TVD scheme', in *Numerical Methods for Partial Differential Equations*, Wiley, New York, 1985.
7. H. C. Yee and P. Kutler, 'Application of second-order accurate, total variation diminishing (TVD) schemes to the Euler equations in general geometries', *NASA TM-85845*, Ames Research Centre, Moffett Field, California, August 1983.
8. G. F. Widhopf, J. C. Buell and E. M. Schmidt, 'Time-dependent near-field muzzle brake flow simulations', *AIAA-82-0973, AIAA/ASME 3rd Joint Thermophysics, Fluids, Plasma and Heat Transfer Conf.* St. Louis, Missouri, 7–11 June 1982.
9. E. M. Schmidt and S. J. Duffy, 'Noise from shock tube facilities', *AIAA-85-0049, AIAA 23rd Aerospace Sciences Meeting*, Reno, Nevada, 14–17 January 1985.
10. B. W. Skews, 'The shape of a diffracting shock wave', *J. Fluid Mech.*, **29**, 297–304 (1967).
11. A. Segev, N. Abuaf and C. Gutfinger, 'Shape of shock waves emerging from a tube', *Israeli J. Technol.*, **13**, 293–299 (1975).
12. A. R. Vick, E. H. Andrews, J. S. Dennard and C. B. Craidon, 'Comparison of experimental free-jet boundaries with theoretical results obtained with the method of characteristics', *NASA Technical Note D-2327 (NTIS N64-23032)*, June 1964.
13. L. N. Howard and D. L. Matthews, 'On the vortices produced in shock diffraction', *J. Appl. Phys.* **27**, (March 1956).
14. Y. J. Moon and H. C. Yee, 'Numerical simulation by TVD schemes of complex shock reflections from airfoils at high angle of attack', *Proc. 25th Aerospace Sciences Meeting*, 12–15 January 1987.
15. C. H. Cooke and K. S. Fansler, 'Numerical simulation of silencers', *Proc. 10th Int. Symp. on Ballistics*, San Diego, CA, 27–28 October 1987.